LETTERS

Electronic measurement and control of spin transport in silicon

Ian Appelbaum[1], Biqin Huang[1] & Douwe J. Monsma[2]

The spin lifetime and diffusion length of electrons are transport parameters that define the scale of coherence in spintronic devices and circuits. As these parameters are many orders of magnitude larger in semiconductors than in metals[1,2], semiconductors could be the most suitable for spintronics. So far, spin transport has only been measured in direct-bandgap semiconductors[3–9] or in combination with magnetic semiconductors, excluding a wide range of non-magnetic semiconductors with indirect bandgaps. Most notable in this group is silicon, Si, which (in addition to its market entrenchment in electronics) has long been predicted a superior semiconductor for spintronics with enhanced lifetime and transport length due to low spin–orbit scattering and lattice inversion symmetry[10–12]. Despite this promise, a demonstration of coherent spin transport in Si has remained elusive, because most experiments focused on magnetoresistive devices; these methods fail because of a fundamental impedance mismatch between ferromagnetic metal and semiconductor[13], and measurements are obscured by other magnetoelectronic effects[14]. Here we demonstrate conduction-band spin transport across 10 μm undoped Si in a device that operates by spin-dependent ballistic hot-electron filtering through ferromagnetic thin films for both spin injection and spin detection. As it is not based on magnetoresistance, the hot-electron spin injection and spin detection avoids impedance mismatch issues and prevents interference from parasitic effects. The clean collector current shows independent magnetic and electrical control of spin precession, and thus confirms spin coherent drift in the conduction band of silicon.

Figure 1a illustrates the operating principle and schematic band diagram of our device. Spin injection and detection is based on the attenuation of minority-spin hot electrons in ferromagnetic thin films, as in spin-valve transistors[15,16]. In our device, the spin-valve transistors used for injection and detection each only have a single ferromagnetic base layer, and we define these as 'hot-electron spin transistors'. In step 1, a solid-state tunnel junction injects unpolarized hot electrons from the Al emitter into the ferromagnetic $Co_{84}Fe_{16}$ base, forming emitter current I_e. Spin-dependent hot-electron scattering attenuates minority spin electrons (step 2), so that the electrons transported over the Schottky barrier and into the undoped single-crystal float-zone (FZ)-Si conduction band (forming injected current I_{c1}, the 'first collector current') are polarized, with their spin parallel to the magnetization of the $Co_{84}Fe_{16}$ (step 3)[17]. After vertical transport through the 10-μm-thick undoped Si (step 4), the spin polarization of the conduction-band electrons is detected by a second hot-electron spin transistor. The $Ni_{80}Fe_{20}$ base again uses ballistic hot-electron spin filtering, so the 'second collector current' (I_{c2}, step 5) formed from ballistic transport through the $Ni_{80}Fe_{20}$ and into the n-Si substrate conduction band is dependent on the relative magnetizations of both ferromagnetic layers. When they are parallel, I_{c2} is higher than when they are antiparallel, but only if electron spin polarization is maintained through the undoped Si layer. Therefore, this device is the electron analogue of the photon polarization-analyser experiment in optics.

There are various intrinsic device aspects that allow a clean spin transport signal in I_{c2}, and that make it immune to fringe field-induced magnetoresistance and Hall effects. (1) The exponential spin selective mean free path dependence in the ferromagnetic films create very large spin polarizations. In principle, this can approach 100%,

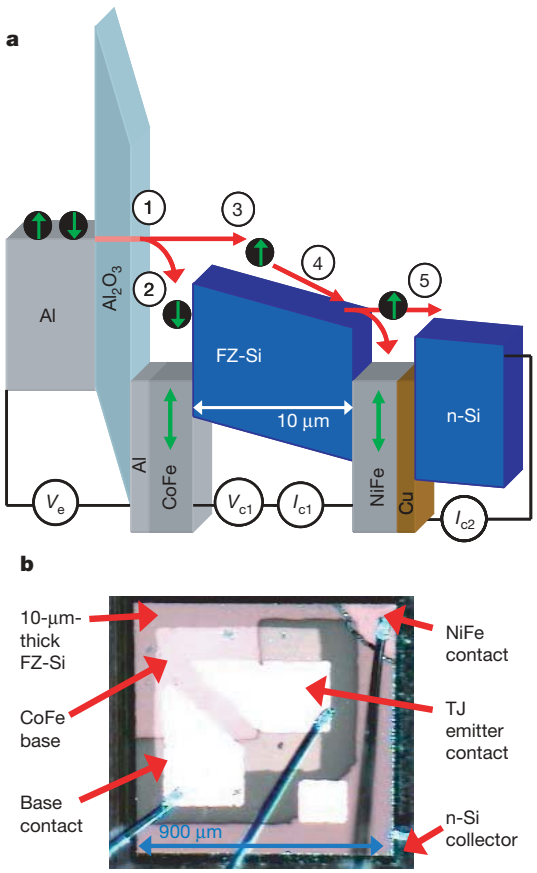

Figure 1 | Illustration of the Si spin transport device. a, Schematic band diagram. At constant emitter voltage (V_e), we measure the 'first collector current' (I_{c1}) at the NiFe contact and 'second collector current' (I_{c2}) at an In contact to the n-Si substrate, under optional voltage bias (V_{c1}) across the single-crystal undoped float-zone Si (FZ-Si) drift region. See text for explanation of sequential transport steps (1)–(5). **b**, A top-down micrograph of a representative wire-bonded Si spin-transport device, showing the device structure, contacts to the spin-injection tunnel junction (TJ) base and emitter, and spin-detector buried NiFe layer.

[1]Department of Electrical and Computer Engineering, University of Delaware, Newark, Delaware 19716, USA. [2]Cambridge NanoTech Inc., Cambridge, Massachusetts 02139, USA.

©2007 Nature Publishing Group

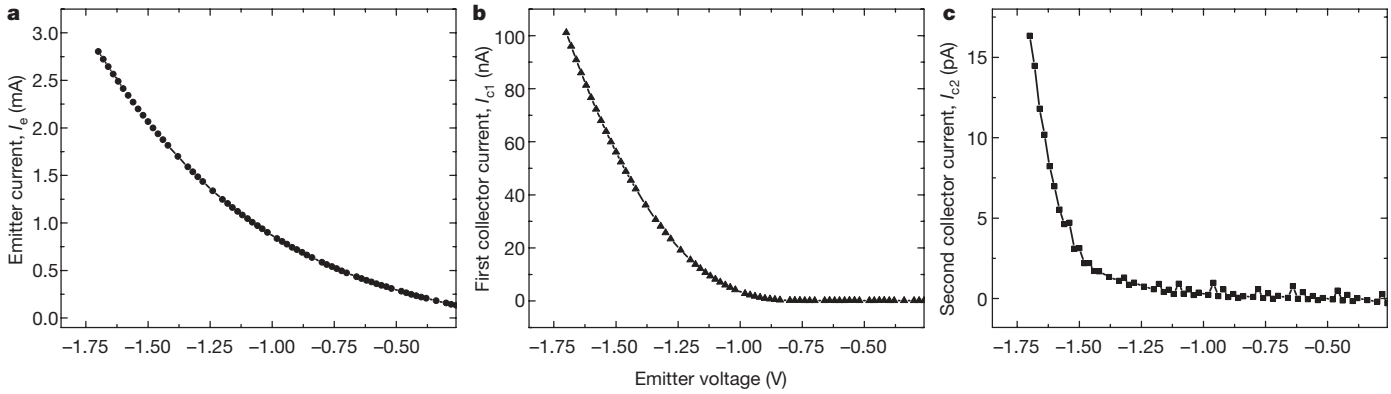

Figure 2 | Simultaneously measured current dependence on tunnel-junction emitter voltage at 85 K. **a**, Emitter current, I_e. **b**, First collector current, I_{c1}, at the $Ni_{80}Fe_{20}$ contact for $V_{c1} = 0$V. **c**, Second collector current, I_{c2}, at an In contact to the n-Si substrate.

allowing effective injection and detection at cryogenic and room temperatures[16]. (2) Because the spin filtering is caused by bulk scattering in the ferromagnetic films, they are easy to reproduce, as there is no interface sensitivity to the spin filtering (as there is, for example, in magnetic tunnel junctions[18]). (3) This device, like a spin-valve transistor, is a high-impedance current source[15,16]. As I_{c2} is driven by I_{c1}, and I_{c1} by I_e, I_{c2} is virtually independent of V_{c1}, the applied voltage across the Si drift region. This also means that any generated Hall voltage in the FZ-Si has no effect on I_{c2}. The underlying background to the insensitivity to resistance and voltage of the FZ-Si is that the potential is screened by the two Schottky barriers on either side, and that the electrons travelling in the FZ-Si conduction band are generated not by an ohmic source, but by hot-electron injection. (4) These devices operate over a wide temperature range, without appreciable change in I_{c2}, despite the fact that the resistivity of undoped Si varies by many orders of magnitude. The insensitivity of I_{c2} to FZ-Si resistance implies that I_{c2} is also insensitive to magnetoresistance in the FZ-Si. In fact, at the temperature we use for measurements here (85 K), the FZ-Si is completely frozen out and its resistivity is $>10^{14}\,\Omega$ cm. This means that there are no thermally or impurity generated electrons, and the only free electrons present are the injected spin polarized electrons.

There are several design aspects that provide our device with a clean spin-transfer current I_{c2}. (1) An undoped FZ-Si device layer is chosen because its extremely low impurity density results in wide Schottky depletion regions and a linear conduction band. This prevents potential wells and long spin dwell times. (2) The device is measured at 85 K to eliminate Schottky leakage currents. (3) Copper (Cu) is used below the $Ni_{80}Fe_{20}$ to provide a low barrier and enable electrons injected by the higher $Si/Ni_{80}Fe_{20}$ Schottky barrier to overcome the Cu/n-Si Schottky barrier. (4) Shape anisotropy of the ferromagnetic films allows us to apply a perpendicular magnetic field for spin precession measurements, without orienting the magnetizations out of plane.

Our fabrication procedures, described in the Methods section, are similar to those of the spin-valve transistor[16], and result in an array of devices like the one wire-bonded and shown in the micrograph displayed in Fig. 1b.

Figure 2a shows the injector tunnel junction current–voltage characteristics, illustrating the expected nonlinear I_e–V_e relationship. Figure 2b shows the simultaneous measurement of injected current I_{c1}–V_e, demonstrating a threshold in I_{c1} at $V_e = -0.8$ V. This represents the 0.8 eV potential energy needed for the electrons to exceed the $Co_{84}Fe_{16}$/FZ-Si Schottky barrier height, and is typical for such metal base transistor-type structures. After vertical transport through 10 μm FZ-Si, some of these electrons travel ballistically through the $Ni_{80}Fe_{20}$/Cu film and into the n-Si collector, resulting in a current (I_{c2}) detected at the In contact to the substrate. This signal rises above our detection limit at an emitter voltage of approximately −1.2 V (Fig. 2c).

In Fig. 3a, in-plane magnetic hysteresis data of I_{c2} at $V_e = -1.8$ V and 85 K are shown. Measurements begin with fully saturated and aligned magnetizations by ramping to our magnetic field maximum. When the magnetic field is swept through zero and changes sign, first the $Ni_{80}Fe_{20}$ switches to align with the field and the magnetizations are antiparallel, resulting in a reduction in I_{c2} of approximately 2%. As the magnetic field passes through the $Co_{84}Fe_{16}$ switching field, the magnetizations again align and the higher collector current is

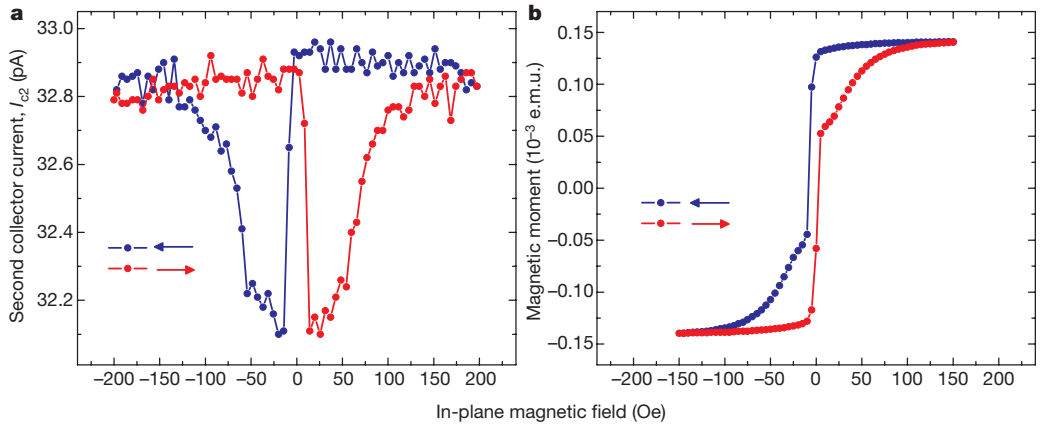

Figure 3 | In-plane magnetic field dependence at 85K. **a**, Second collector current, I_{c2}, at constant emitter bias $V_e = -1.8$ V and $V_{c1} = 0$ V, showing a clear ~2% spin-valve effect. **b**, SQUID magnetometer measurements, showing switching fields consistent with the behaviour seen in **a**. Arrows indicate magnetic field sweep direction.

©2007 Nature Publishing Group

regained by approximately 125 Oe, consistent with the magnetic hysteresis data shown in Fig. 3b. The symmetric magnetic-field dependence of I_{c2} upon reversal of sweep direction in Fig. 3a indicates that the electron spin maintains polarization while travelling through 10 μm of FZ-Si. Results similar to Fig. 3a are also found when the emitter tunnel junction is operated in constant current mode, and many devices have consistently been measured with substantially similar results.

In Fig. 4a, we show the dependence of I_{c2} on magnetic field perpendicular to the film plane with $V_{c1} = 0$ V. The measurement begins with the field at −5,000 Oe, where a small in-plane component is sufficient to saturate the in-plane $Ni_{80}Fe_{20}$ and $Co_{84}Fe_{16}$ magnetizations in a parallel configuration. Following the red line to the right towards smaller field values, we notice a peak near −700 Oe and a dip near −350 Oe. Once the magnetic field increases towards positive values past zero, the small in-plane component of external magnetic field switches the $Ni_{80}Fe_{20}$ magnetization, causing an antiparallel magnetization configuration and inverting the magnitudes of the oscillation. Reversing the field scan direction (blue line) results in similar features reflected on the magnetic field axis, but with a deeper dip at small negative field due to sharper $Ni_{80}Fe_{20}$ switching in that direction.

Although $V_{c1} = 0$ V in Fig. 4a, a vertical drift field (due to a voltage drop caused by emitter current flowing through the $Al/Co_{84}Fe_{16}$ thin base film) exists in the FZ-Si. Under these conditions, where drift is the primary transport mechanism, the magnetic fields of the extrema seen in Fig. 4a can be identified approximately as the conditions for π and 2π precession. The precessing spin direction, projected on the measurement axis defined by the $Ni_{80}Fe_{20}$ magnetization, causes oscillation in I_{c2}.

Because of the action of random diffusion, spin dephasing occurs with higher precession angles, and results in damped higher-order oscillations (Hanle effect)[19]. Therefore, just two multiples of π precession angle are seen. A useful advantage of the four-terminal design

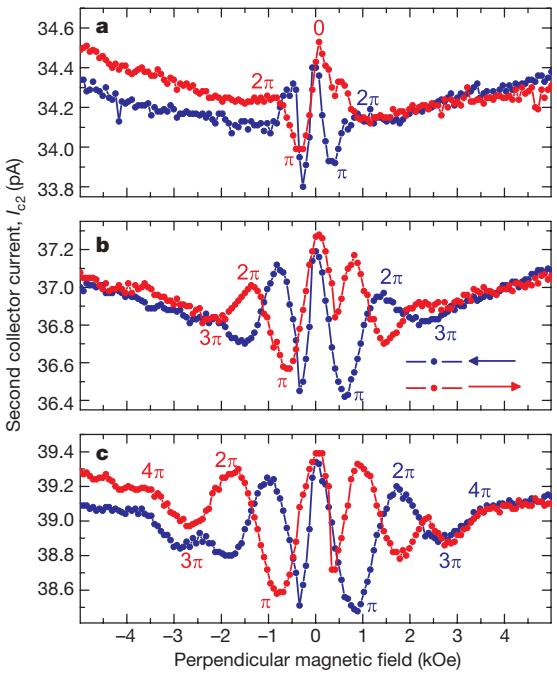

Figure 4 | Spin precession and dephasing in a perpendicular magnetic field at constant emitter voltage $V_e = -1.8$ V and 85 K. a, Second collector current, I_{c2}, in zero applied voltage V_{c1}. **b**, **c**, As **a** but under an accelerating voltage bias of 0.5 V (**b**) and of 1.0 V (**c**). At higher accelerating voltages, the spin polarized electron transport time is reduced in the increased drift field, so the precession angle at fixed magnetic field is smaller, causing an increased precession period and revealing the presence of precession angles up to 4π.

and rectifying Schottky barriers on either side of the FZ-Si in our device is that I_{c2} is virtually independent of voltage across the drift region. Therefore, the drift electric field can be tuned to change the spin polarized electron transit time between injection and detection with applied voltage V_{c1}. When the electric drift field is increased with an applied voltage bias, the transit time is reduced, and the precession angle at any fixed magnetic field is consequently also reduced. This pushes the extrema to higher values of perpendicular magnetic fields, clearly shown in Fig. 4b and c at respectively 0.5 V and 1.0 V accelerating voltage. Under these conditions of higher accelerating electric field, drift is even more dominant than in Fig. 4a, and precession angles up to 4π can be seen. The precession extrema for parallel magnetization configurations are labelled with their precession angle in Fig. 4a–c. In this way, maxima correspond to even multiples of π and minima correspond to odd multiples of π. The large number of precession extrema and their expected electric field dependence are conclusive evidence of strong coherent spin transport in the FZ-Si.

Using the spin precession frequency $g\mu_B/h = 2.8\,\mathrm{MHz\,Oe^{-1}}$ (where g is the electron spin g-factor, μ_B is the Bohr magneton, and h Planck's constant; ref. 20), the transit time can be calculated from the magnetic field value of the first extremum, where the average precession angle is approximately π rad. Using ±350 Oe as the position of the extrema in Fig. 4a, we have $\tau_{transit} = \pi/(2\pi \times 2.8 \times 10^6 \times 350) \approx 0.5$ ns, which gives an approximately $2 \times 10^6\,\mathrm{cm\,s^{-1}}$ drift velocity through the 10-μm-thick FZ-Si[21]. The positions of the precession extrema in Fig. 4b and c indicate transit times of ~0.3 ns and ~0.2 ns, respectively.

As the electron transit time e is controlled by applied voltage V_{c1}, the normalized magnetocurrent change in I_{c2} (ΔI_{c2}) can be used to deduce the spin lifetime in FZ-Si. Assuming a simple exponential decay law, and using the measured transit times from Fig. 4a–c, we can calculate the spin lifetime τ_{sf} (at 85 K) using ratios of

$$\frac{\Delta I_{c2}(V_{c1})}{I_{c1}(V_{c1})} \propto \exp\left[-\frac{\tau_{transit}(V_{c1})}{\tau_{sf}}\right]$$

for each pair of data. With the maximum fluctuations shown in Fig. 4a–c, and using simultaneously-measured $I_{c1}(0\mathrm{V}) = 118$ nA, $I_{c1}(0.5\mathrm{V}) = 132$ nA and $I_{c1}(1.0\mathrm{V}) = 139$ nA, we calculate $\tau_{sf} \approx 1$ ns. This value is consistent with spin lifetimes in the direct-bandgap semiconductor GaAs measured at similar temperatures using optical techniques[3]. However, we must consider this value a lower bound, with the actual lifetime potentially much longer:[22] the applied voltage V_{c1} could alter the magnetocurrent magnitude ΔI_{c2} separately from the finite spin lifetime and variable transit time effect, artificially reducing our estimate.

It is possible to use alternative spin injection schemes with our detection method, such as direct tunnel injection[23–25]. However, in that case the injection current is not decoupled from drift field and thus independent control of spin precession by magnetic field and electric drift field is compromised; on the other hand, the total signal will be larger. Finally, we hope that our hot-electron injection/detection scheme will be implemented in lateral geometries, to advance the development of future spin-based integrated circuits.

METHODS

Room-temperature ultrahigh-vacuum wafer bonding[16] is used to assemble the semiconductor–metal–semiconductor spin detection structure. First, a 4-nm-thick Cu film is deposited via thermal evaporation on a 1 Ω cm 50-mm-diameter n-Si wafer to achieve a low second collector Schottky barrier. Then, during deposition of 2 nm of $Ni_{80}Fe_{20}$ on both this wafer and on a 50-mm-diameter silicon-on-insulator (SOI) wafer with a 10 μm undoped single-crystal FZ-Si device layer, the wafers are pressed together *in situ*, forming a cohesive bond and a single 4-nm-thick $Ni_{80}Fe_{20}$ film. Transmission electron microscopy analysis of similarly bonded interfaces is shown in ref. 16. After SOI substrate removal and mesa patterning using the 2-μm-thick buried oxide as a mask, a tunnel junction structure is deposited using electron beam deposition of a 5 nm $Co_{84}Fe_{16}$ and 5 nm Al bilayer base (500 μm × 500 μm) and (after ultraviolet

©2007 Nature Publishing Group

ozone oxidation to form the tunnel barrier) two Al contacts. For isolation, a wafer saw is used to cut trenches partially through the n-Si collector substrate, forming an array of devices each 900 μm × 900 μm.

Pinholes in these deposited layers cannot result in spurious measurements of I_{c2}: (1) if they exist in the tunnel oxide, the emitter tunnel junction is shorted and the device is clearly inoperable; (2) if they exist in the Al/$Co_{84}Fe_{16}$ layer, the emitter forms a rectifying Schottky barrier there and the device is unaffected; and (3) pinholes in the single-crystal FZ-Si layer are not possible.

As fabricated, the two Al contacts both form tunnel junctions with the Al/$Co_{84}Fe_{16}$ base. Ramping a current source through them in series breaks one and leaves the other intact. Contact for I_{c1} is to the $Ni_{20}Fe_{80}$ buried layer, and contact for I_{c2} is with cold-pressed indium to the n-Si substrate. This current has been measured with a Keithley 236 source-measure unit, without any other additions or special efforts.

Received 22 December 2006; accepted 30 March 2007.

1. Jedema, F. J., Heersche, H. B., Filip, A. T., Baselmans, J. J. A. & van Wees, B. J. Electrical detection of spin precession in a metallic mesoscopic spin valve. *Nature* **416,** 713–717 (2002).
2. Valenzuela, S. O. & Tinkham, M. Direct electronic measurement of the spin Hall effect. *Nature* **442,** 176–179 (2006).
3. Kikkawa, J. M. & Awschalom, D. D. Resonant spin amplification in n-type GaAs. *Phys. Rev. Lett.* **80,** 4313–4316 (1998).
4. Kikkawa, J. M. & Awschalom, D. D. Lateral drag of spin coherence in gallium arsenide. *Nature* **397,** 139–141 (1999).
5. Kato, Y., Myers, R. C., Gossard, A. C. & Awschalom, D. D. Coherent spin manipulation without magnetic fields in strained semiconductors. *Nature* **427,** 50–53 (2003).
6. Stephens, J. *et al.* Spin accumulation in forward-biased MnAs/GaAs Schottky diodes. *Phys. Rev. Lett.* **93,** 097602 (2004).
7. Crooker, S. A. *et al.* Imaging spin transport in lateral ferromagnet/ semiconductor structures. *Science* **309,** 2191–2195 (2005).
8. Lou, X. *et al.* Electrical detection of spin accumulation at a ferromagnet-semiconductor interface. *Phys. Rev. Lett.* **96,** 176603 (2006).
9. Lou, X. *et al.* Electrical detection of spin transport in lateral ferromagnet–semiconductor devices. *Nature Phys.* **3,** 197–202 (2007).
10. Zutic, I., Fabian, J. & Erwin, S. C. Spin injection and detection in Si. *Phys. Rev. Lett.* **97,** 026602 (2006).
11. Zutic, I., Fabian, J. & Das Sarma, S. Spintronics: Fundamentals and applications. *Rev. Mod. Phys.* **76,** 323–410 (2004).
12. Tyryshkin, I. M., Lyon, S. A., Astashkin, A. V. & Raitsimring, A. M. Electron spin relaxation times of phosphorus donors in Si. *Phys. Rev. B* **68,** 193207 (2003).
13. Schmidt, G., Ferrand, D., Molenkamp, L. W., Filip, A. T. & van Wees, B. J. Fundamental obstacle for electrical spin injection from a ferromagnetic metal into a diffusive semiconductor. *Phys. Rev. B* **62,** R4790–R4793 (2000).
14. Monzon, F. G., Tang, H. X. & Roukes, M. L. Magnetoelectronic phenomena at a ferromagnet-semiconductor interface. *Phys. Rev. Lett.* **84,** 5022–5022 (2000).
15. Monsma, D. J., Lodder, J. C., Popma, ThJA & Dieny, B. Perpendicular hot electron spin-valve effect in a new magnetic field sensor: The spin valve transistor. *Phys. Rev. Lett.* **74,** 5260–5263 (1995).
16. Monsma, D. J., Vlutters, R. & Lodder, J. C. Room temperature-operating spin-valve transistors formed by vacuum bonding. *Science* **281,** 407–409 (1998).
17. Jiang, X. *et al.* Optical detection of hot-electron spin injection into GaAs from a magnetic tunnel transistor source. *Phys. Rev. Lett.* **90,** 256603 (2003).
18. Zega, T. J. *et al.* Determination of interface atomic structure and its impact on spin transport using Z-contrast microscopy and density-functional theory. *Phys. Rev. Lett.* **96,** 196101 (2006).
19. Johnson, M. & Silsbee, R. H. Interfacial charge-spin coupling: Injection and detection of spin magnetization in metals. *Phys. Rev. Lett.* **55,** 1790–1793 (1985).
20. Portis, A. M., Kip, A. F., Kittel, C. & Brattain, W. H. Electron spin resonance in a silicon semiconductor. *Phys. Rev.* **90,** 988–989 (1953).
21. Jacoboni, C., Canali, C., Ottaviani, G. & Quaranta, A. A. A review of some charge transport properties of Si. *Solid State Electron.* **20,** 77–89 (1977).
22. Tyryshkin, A. M., Lyon, S. A., Jantsch, W. & Schäffler, F. Spin manipulation of free two-dimensional electrons in Si/SiGe quantum wells. *Phys. Rev. Lett.* **94,** 126802 (2005).
23. Jiang, X. *et al.* Highly spin polarized room temperature tunnel injector for semiconductor spintronics using MgO (100). *Phys. Rev. Lett.* **94,** 056601 (2005).
24. Smith, D. L. & Silver, R. N. Electrical spin injection into semiconductors. *Phys. Rev. B* **64,** 045323 (2002).
25. Hanbicki, A. T., Jonker, B. T., Itskos, G., Kioseoglou, G. & Petrou, A. Efficient electrical spin injection from a magnetic metal/tunnel barrier contact into a semiconductor. *Appl. Phys. Lett.* **80,** 1240–1242 (2002).

Acknowledgements We acknowledge assistance during fabrication from I. Altfeder, SQUID measurements by G. Hadjipanayis and A. Gabay, and use of the wafer saw from K. Goossen. This work is supported by ONR and DARPA/MTO.

Author Information Reprints and permissions information is available at www.nature.com/reprints. The authors declare no competing financial interests. Correspondence and requests for materials should be addressed to I.A. (appelbaum@ee.udel.edu).

©2007 Nature Publishing Group